SAND2013-10593C

Backprojection for GMTI processing

A. W. Doerry*

Sandia National Laboratories, P.O. Box 5800, MS 0519, Albuquerque, NM 87185

ABSTRACT

Backprojection has long been applied to SAR image formation. It has equal utility in forming the range-velocity maps for Ground Moving Target Indicator (GMTI) radar processing. In particular, it overcomes the problem of targets migrating through range resolution cells.

Keywords: radar, GMTI, backprojection

1 INTRODUCTION

Backprojection (BP), a.k.a. Filtered Backprojection (FBP), or Convolution Backprojection (CBP), has its roots in tomography, but has been applied to Synthetic Aperture Radar (SAR) processing for some time. Perhaps the earliest observation of this relationship was by Munson, et al.[1] Its attractiveness is that the SAR image reconstruction is not limited by issues that plague common range-Doppler transform techniques, such as range migration or spatially variant phase errors, etc.

While BP has often been applied to SAR image formation, and even investigated for image formation of moving targets, the literature seems somewhat sparse regarding its application to the basic Ground Moving Target Indicator (GMTI) radar detection process. We note that conventionally, GMTI processing requires forming a range-velocity map where the velocity analysis is done with Fourier Techniques. Historically this has been quite adequate, except when the spread of potential target velocities causes excessive range migration during a Coherent Processing Interval (CPI).

The basic problem is when a target migrates farther during a CPI than the range resolution of the radar data, then the target echo energy smears in range and diminishes in Signal to Noise Ratio (SNR), thereby decreasing likelihood of detection. This is particularly problematic when range resolution becomes rather fine, as with High-Range-Resolution (HRR) modes. These modes are becoming increasingly popular to facilitate feature-aided trackers and vehicle classification techniques.

A solution for mitigating excessive range-migration during a CPI was proposed by Perry, et al., [2,3] where they resample the 'keystone' nature of the data in the Fourier-space of the range-velocity map in a manner similar to the polar-reformatting required during SAR image formation using the Polar-Format Algorithm (PFA). This allows better 'focusing' of the target, with the desirable side effect of increasing SNR.

Herein we propose and show how BP can be used to directly create the range-velocity map, thereby mitigating residual range migration. This paper summarized an earlier report on this topic.[4]

For a basic reference on GMTI performance we refer the reader to a report by Doerry.[5]

* awdoerr@sandia.gov; phone 505-845-8165; www.sandia.gov/radar

2 THE DATA MODEL

We will assume that the data set (raw data from a collection of pulses) for a CPI has been range-compressed such that it can be modeled by

$$X(k,n) = A_R W_{I_{TX}}\left(\frac{a_{wr}}{\rho_r}\left(\delta_r k - s_{r,n}\right)\right)\exp j\left\{-\frac{2\omega_0}{c}s_{r,n}\right\}. \tag{1}$$

where

c = velocity of propagation,
A_R = received signal amplitude (after compression),
k = range-compressed data index, $-K/2 \le k < K/2$,
n = pulse sample index within a CPI, $-N/2 \le n < N/2$,
I_{TX} = length of the received pulse in samples (prior to range compression),
ω_0 = nominal constant reference frequency for the CPI in rad/sec,
$s_{r,n}$ = nominal relative range between scatterer and range-swath center,
δ_r = slant-range pixel spacing,
ρ_r = slant-range resolution. (2)

During the range-compression processing, spectral data tapering was employed for sidelobe control, where we identify a generic window function and its Discrete Fourier Transform (DFT), or Impulse Response (IPR), as follows.

$w_U(u)$ = window function, $-U/2 \le u < U/2$, and
$W_U(v) = DFT_{V,u}(w(u))$ = the IPR of the window function, $-V/2 \le v < V/2$. (3)

We shall also characterize the mainlobe width of $W_U(v)$ for the window taper used in range processing with

a_{wr} = the normalized broadening factor for the mainlobe in range. (4)

This broadening factor is measured at the −3 dB width of the IPR mainlobe. The window function is zero outside of its defined range. We will also generally assume (or insist) that the DC gain of the window function is *U*. What this really means is that if we sum all the window function weights, the result is *U*, and its IPR has peak magnitude of *U*.

What we have at this point is range-compressed data for each pulse. What we don't have yet is any results of processing across multiple pulses. Before we do this, we need to characterize how targets behave across multiple pulses within a CPI. The intent will be to characterize target velocity. We will henceforth call this velocity processing.

The object of velocity processing is to coherently combine multiple range-compressed pulse data vectors, both to enhance SNR and to estimate the target's component of the line-of-sight velocity. Accordingly, we identify some basic timing and control parameters as

f_p = Pulse Repetition Frequency (PRF) of the radar, and
N = number of pulses in a CPI. (5)

Note that the center of the CPI corresponds to index $n = 0$. We will furthermore define the following relevant geometric parameters as

$\theta_{s,n}$ = the squint angle for the n^{th} pulse, with $-\pi \le \theta_{s,n} < \pi$. (6)

This squint angle is with respect to the radar's velocity vector as projected onto the ground. We incorporate pulse-to-pulse range variations of an echo by expanding

$$s_{r,n} = s_{r,0} - v_{los,0} T_p n \,. \tag{7}$$

where

$s_{r,0}$ = target range offset for $n = 0$,

$v_{los,0}$ = line-of-sight closing velocity for $n = 0$, and

$T_p = \dfrac{1}{f_p}$ = the Pulse Repetition Interval (PRI). (8)

The range-compressed data model modified to incorporate pulse-to-pulse relative radar to target motion becomes

$$X(k,n) = A_R \, W_{I_{TX}} \left(\frac{a_{wr}}{\rho_r} \left(\delta_r k - \left(s_{r,0} - v_{los,0} T_p n \right) \right) \right) \exp j \left\{ -\frac{2\omega_0}{c} \left(s_{r,0} - v_{los,0} T_p n \right) \right\}. \tag{9}$$

We note that CPI pulse index *n* appears in two places.

1. The manifestation of index *n* in the range IPR magnitude (inside $W_{I_{TX}}(\,)$) indicates that the position of the mainlobe peak migrates with pulse index *n*. This pulse-to-pulse magnitude peak variation is typically referred to as 'range migration'.
2. The manifestation of index *n* in the range IPR phase (argument of the exponential) indicates that the phase of the compressed pulse ramps with *n*. This pulse-to-pulse phase variation is typically referred to as 'Doppler'.

A stationary (with respect to the target scene) object in the direction of the azimuthal boresight of the antenna will exhibit a closing velocity with the radar calculated as

$$v_{clutter,n,k} = v_a \cos\theta_{s,n} \cos\psi_{d,k} \,, \tag{10}$$

where

$\psi_{d,k}$ = depression angle with respect to horizontal. (11)

We use the term "clutter" to reference generally uninteresting and nominally stationary echo returns in the target scene, or field of view. After all, for GMTI we are interested in targets moving with respect to their stationary surroundings. Note that the radar closing velocity with respect to clutter does depend on slant-range via the variation in depression angle. For this reason we have now included the slant-range index *k* in the subscript of the depression angle.

Typical CPI lengths for GMTI are a small fraction of a second, often 0.1 seconds or so.[5] Larger CPI lengths often begin to interfere with target coherence. We will make the assumption that during a CPI, we may use the clutter velocity that corresponds to the center of the CPI, that is, we may assume

$$v_{clutter,n,k} \approx v_{clutter,0,k} = v_a \cos\theta_{s,0} \cos\psi_{d,k} \,. \tag{12}$$

Furthermore, we recall that $v_{los,0}$ is the closing velocity between the radar and a potentially moving target when $n = 0$. We will also assume that the target's component of the line-of-sight velocity is constant during a CPI. The total line-of-sight velocity then becomes dependent on range. Consequently we also now add to the line-of-sight velocity a subscript *k* to signify the range dependence. This yields the combined line-of-sight velocity as

$$v_{los,0,k} = v_{clutter,0,k} + v_{target} \,. \tag{13}$$

This lets us further refine our range-compressed data model to

$$X(k,n) \approx A_R \, W_{I_{TX}} \left(\frac{a_{wr}}{\rho_r} \left(\delta_r k - \begin{pmatrix} s_{r,0} - v_{clutter,0,k} T_p n \\ -v_{target} T_p n \end{pmatrix} \right) \right) \exp j \left\{ -\frac{2\omega_0}{c} \begin{pmatrix} s_{r,0} - v_{clutter,0,k} T_p n \\ -v_{target} T_p n \end{pmatrix} \right\}. \tag{14}$$

Expanding the clutter velocity will yield the expression

$$X(k,n) \approx \left[\begin{array}{l} A_R \, W_{I_{TX}} \left(\frac{a_{wr}}{\rho_r} \left(\delta_r k - \begin{pmatrix} s_{r,0} - v_a \cos\theta_{s,0} \cos\psi_{d,k} T_p n \\ -v_{target} T_p n \end{pmatrix} \right) \right) \\ \times \exp j \left\{ -\frac{2\omega_0}{c} \begin{pmatrix} s_{r,0} - v_a \cos\theta_{s,0} \cos\psi_{d,k} T_p n \\ -v_{target} T_p n \end{pmatrix} \right\} \end{array} \right]. \tag{15}$$

With this model, the task at hand becomes to coherently combine the multiple pulses to enhance SNR and estimate target velocity. To do so properly means accounting for the velocity of both the radar and the target. The radar velocity is presumed to be known, but the target velocity is not. Consequently, the pulses need to be combined for a variety of different target velocities to determine which yields the 'best' solution. From this we can also identify the target line-of-sight velocity component.

We propose to back-project this data onto a grid of range versus target-velocity. However, before doing this, some comments are in order.

- Even for fairly fine range resolution, the resolution bandwidth is typically small compared to the center frequency. Consequently, there is no need to 'filter' the data as in 'Filtered' BP. That is, there is no need to scale the frequency content of the data.
- Often, we will desire to perform some radiometric correction of the data by adjusting amplitude as a function of range to compensate for range losses and antenna elevation pattern effects. While we note that this is desirable, and in fact rather simple to implement, we will treat this as beyond the scope of this report and not discuss it further.
- The relationship of slant-range offset to depression angle for GMTI targets will depend on the topography of the ground. We will assume a flat earth, for now.
- Recall that the IPR oversampling factor is calculated as

$$a_{osr} = \frac{\rho_r}{\delta_r} \,. \tag{16}$$

  Later, during velocity processing itself, we will need to interpolate the range-compressed data to arbitrary locations. This will be considerably easier (less complicated) with large oversampling factors in the range compressed data. This means selecting, if possible, a range-spacing δ_r on the small side.

3 VELOCITY PROCESSING

The object of velocity processing is to create a range-velocity 'image' suitable for the target detection process, often implemented with Constant False Alarm Rate (CFAR) algorithms on the magnitude of the range-velocity image. The range-compressed data vector model is repeated here as

$$X(k,n) \approx \left[\begin{array}{l} A_R \, W_{I_{TX}} \left(\dfrac{a_{wr}}{\rho_r} \left(\delta_r k - \left(\begin{array}{l} s_{r,0} - v_a \cos\theta_{s,0} \cos\psi_{d,k} T_p n \\ -v_{target} T_p n \end{array} \right) \right) \right) \\ \times \exp j \left\{ -\dfrac{2\omega_0}{c} \left(\begin{array}{l} s_{r,0} - v_a \cos\theta_{s,0} \cos\psi_{d,k} T_p n \\ -v_{target} T_p n \end{array} \right) \right\} \end{array} \right]. \quad (17)$$

We now wish to create an 'image' of this data. That is, we wish to see how this target echo response manifests in a 2-D array of image sample locations, with dimensions range and target-velocity relative to clutter. The data has been range-compressed. Now we need to perform the "backprojection" part of the algorithm. The essence of BP image formation is now the following backprojection procedure, also illustrated in Figure 1.

1. Create a grid of image sample range/velocity pairs, and
2. Process the range-compressed data to the image sample grid, one pulse at a time.

The processing itself requires that for each pulse of collected data *n*, and for each sample range/velocity pair in the image sample grid, we apply the following operations, also illustrated in Figure 2.

a. Calculate range difference between image sample range/velocity and the reference range,
b. Calculate the corresponding fractional range difference index *k'*,
c. Interpolate the data vector to the fractional range difference index *k'*,
d. Compensate for the Doppler phase term, and
e. Accumulate the interpolated value into the target image array.

3.1 Creating the 'Image' Sample Grid

We shall presume to form a typical range-velocity 'image' that is a 2-D map of radar reflectivity. We shall further presume that the image is a rectangular grid of sample locations centered on the reference range and reference target velocity that is also the expected stationary clutter velocity. Neither of these presumptions is mandatory for BP image formation, but both are nevertheless convenient for us. In any case, we presume that the image rectangular grid array may be expressed with

$$\begin{aligned} \hat{v}_r &= u_v \delta_v \text{ = velocity-dimension offset, and} \\ \hat{s}_r &= u_s \delta_s \text{ = slant-range-dimension offset.} \end{aligned} \quad (18)$$

where

$$\begin{aligned} u_v &= \text{velocity-dimension index, with } -U_v/2 \le u_v < U_v/2, \\ u_s &= \text{slant-range-dimension index, with } -U_s/2 \le u_s < U_s/2, \\ \delta_v &= \text{velocity-dimension pixel spacing, and} \\ \delta_s &= \text{slant-range-dimension pixel spacing.} \end{aligned} \quad (19)$$

The image size in the ground-plane would then have dimensions

$$\begin{aligned} D_v &= U_v \delta_v \text{ = velocity-dimension image size in units of velocity, and} \\ D_s &= U_s \delta_s \text{ = slant-range-dimension image size.} \end{aligned} \quad (20)$$

In addition, we will need to relate the clutter velocity term to the slant range. Recall that

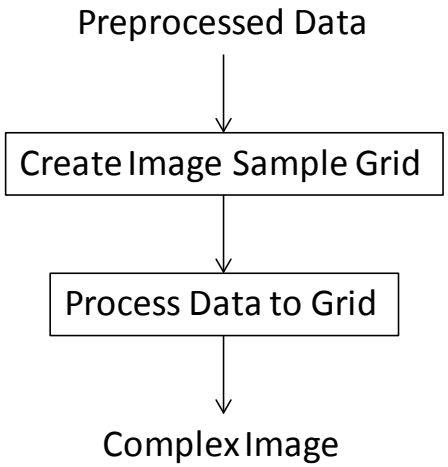

Figure 1. Basic Backprojection procedure.

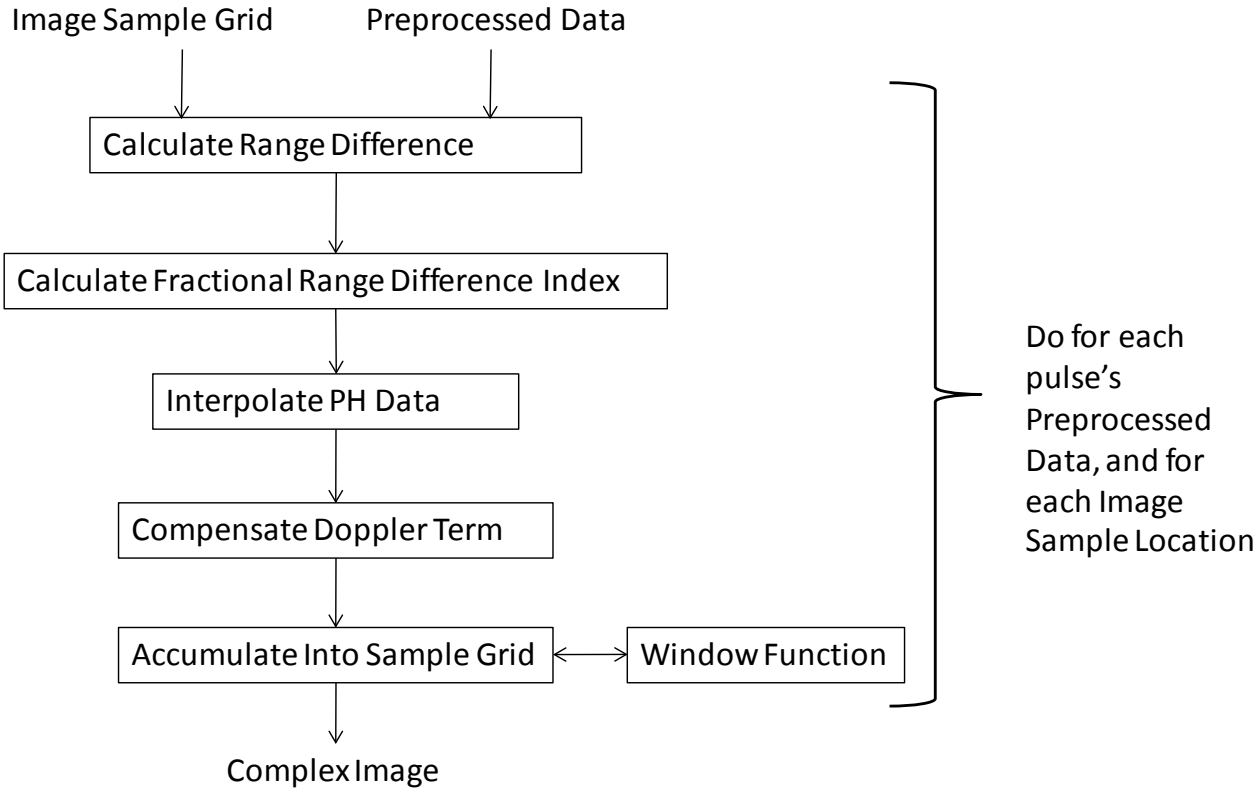

Figure 2. Detailed Backprojection processing steps.

$$v_{clutter,0,k} = v_a \cos\theta_{s,0} \cos\psi_{d,k} \,. \tag{21}$$

The range-dependent term is clearly the depression angle component of this expression. For a flat earth model, we may calculate

$$\psi_{d,k} = \operatorname{asin}\left(\frac{h_a}{r_{c0} + \hat{s}_r} \right). \tag{22}$$

where

$$\begin{aligned} h_a &= \text{ height of radar above target reference altitude, and} \\ r_{c0} &= \text{ reference slant-range of radar to center swath.} \end{aligned} \tag{23}$$

With knowledge of the local topography, for example with Digital Terrain Elevation Data (DTED), we may have the possibility of using a *z*-dimension offset for each slant range. That is, we might allow calculating

$$\hat{s}_z = DTED\left(\hat{s}_r\right) = z\text{-dimension (height) offset.} \tag{24}$$

Now, with each slant range we can identify a depression angle that is target height dependent, namely

$$\psi_{d,k} = \operatorname{asin}\left(\frac{h_a - \hat{s}_z}{r_{c0} + \hat{s}_r} \right). \tag{25}$$

The underlying assumption here is that the target is on the ground. Of course, topography may also vary with azimuthal offset from the clutter center-line. We offer the following comments with respect to this.

- We stipulate, however, that a typical GMTI system operates with a fan-beam with a ground footprint that has a much larger extent in range than in azimuth. Consequently the potential variation of target height with range would seem to be more problematic than with azimuth position within the beam.
- A single-channel GMTI system has no mechanism to reliably discern azimuthal position offset for a moving target anyway. If terrain knowledge were available to know the variation with azimuth, we would have to average it in some fashion or otherwise develop a single representative value anyway.
- Multi-aperture GMTI systems may allow some ability to calculate target azimuthal offset and correct target velocity and position accordingly. This is beyond the scope of this report.

We further note that

$$\cos\psi_{d,k} = \cos\left(\operatorname{asin}\left(\frac{h_a - \hat{s}_z}{r_{c0} + \hat{s}_r} \right) \right) = \sqrt{1 - \left(\frac{h_a - \hat{s}_z}{r_{c0} + \hat{s}_r} \right)^2} \,. \tag{26}$$

3.2 Process the Data to the Image Sample Grid

In this section we step through the process displayed in Figure 2. That is, for each preprocessed received echo pulse data with index *n*, we engage the following steps for each image location index pair $\left(u_v, u_s\right)$.

3.2.1 Calculate Range Difference Between Image Sample Location and Reference Range/Velocity

Recall that with each index pair (u_v, u_s) we can identify a unique range-velocity coordinate $(\hat{v}_r, \hat{s}_r)$. Therewith we are able to calculate the range to the radar at pulse index *n*, and in particular wish to calculate the range difference between the image sample location and the reference range/velocity as

$$\hat{s}_{r,n} = \hat{s}_r - v_a \cos\theta_{s,0} \cos\psi_{d,k} T_p n - \hat{v}_r T_p n . \tag{27}$$

3.2.2 Calculate the Fractional Range Difference Index *k'*

With a range difference $\hat{s}_{r,n}$ we can now calculate the corresponding non-integer effective index value as

$$k' = \frac{\hat{s}_{r,n}}{\delta_r} . \tag{28}$$

This can be expanded in terms of the other indices to

$$k' = \frac{1}{\delta_r}\left(u_s \delta_s - v_a \cos\theta_{s,0} \left(\sqrt{1 - \left(\frac{h_a - \hat{s}_z}{r_{c0} + u_s \delta_s} \right)^2} \right) T_p n - u_v \delta_v T_p n \right) . \tag{29}$$

3.2.3 Interpolate the Data Vector to the Fractional Range Difference Index *k'*

This step essentially accommodates range migration. Given the preprocessed data vector $X(k,n)$ over index values *k*, we wish to calculate the interpolated value $X(k',n)$ at a specific effective index value *k'*, which results in the data model given by

$$X(k',n) = A_R W_{I_{TX}} \left(\frac{a_{wr}}{\rho_r} \left(\delta_r k' - s_{r,n} \right) \right) \exp j\left\{ -\frac{2\omega_0}{c} s_{r,n} \right\} . \tag{30}$$

Note that for any one pulse *n*, and any one image location (u_v, u_s), the entity $X(k',n)$ is just one complex number.

Radar data interpolation is a rich topic. There is definitely a science to it, meaning that interpolation algorithm details need to be chosen with purpose, else undesired artifacts in the image are likely. A thorough discussion of interpolation is beyond the scope of this report, but good insight can be had in a paper by Doerry, et al.[6]

3.2.4 Compensate for the Doppler Phase Term

This step focuses the data to the range/velocity combination $(\hat{v}_r, \hat{s}_r)$. We do this by correcting the phase of $X(k',n)$ by multiplying this particular sample as follows.

$$X'(k',n) = X(k',n) \exp j\left\{ +\frac{2\omega_0}{c} \hat{s}_{r,n} \right\} . \tag{31}$$

Multiplying this out yields the model

$$X'(k',n) = A_R W_{I_{TX}} \left(\frac{a_{wr}}{\rho_r} \left(\delta_r k' - s_{r,n} \right) \right) . \tag{32}$$

3.2.5 Accumulate the Interpolated Value Into the Target Array

This is the step that adds this data into the image array at index location (u_v, u_s). So, when all is said and done, the image formation process is the accumulation of data into the image grid, over all pulses and for each image sample grid location. We describe this resulting complex range-velocity map ('image') as a collection of pixels where an individual pixel value is calculated as

$$Z(u_v, u_s) = \sum_n X'(k', n). \tag{33}$$

Window Functions for Sidelobe Control

We note that in the accumulation of processed data into the target array, all pulses contribute equally to the accumulation, resulting in a characteristic sinc() function in the IPR in the velocity dimension, with the attendant generally unacceptable sidelobes. To reduce sidelobes, we need to employ a weighted summation, with a taper over index *n*.

$$Z(u_v, u_s) = \sum_n w_N(n) X'(k', n). \tag{34}$$

We state without elaboration that for large range dimensions, we may at times wish to equalize velocity resolutions as a function of range by adjusting window parameters as a function of range.

4 THE RANGE-VELOCITY IMAGE MODEL

The output of the previous image formation operations is a 2-dimensional array of data, with dimensions of velocity and range, with indices (u_v, u_s). While the proper steps have been defined, it remains somewhat unclear what the output 'image' looks like. Accordingly, we can gain some insight into the image by expanding the previous result to

$$Z(u_v, u_s) = \sum_n w_N(n) X(k', n) \exp j\left\{+\frac{2\omega_0}{c}\hat{s}_{r,n}\right\}. \tag{35}$$

We note that for expected CPI lengths we can approximate for our purposes here

$$k'\delta_r \approx u_s \delta_s. \tag{36}$$

This allows us to further expand and approximate

$$Z(u_v, u_s) = \sum_n A_R W_{I_{TX}}\left(\frac{a_{wr}}{\rho_r}\left(u_s\delta_s - s_{r,0}\right)\right) w_N(n) \exp j\left\{-\frac{2\omega_0}{c}\left(u_v\delta_v - v_{target}\right)T_p n\right\}. \tag{37}$$

Remember that we are not engaging any processing steps here, but merely performing some mathematical operations to understand the nature of the result. By performing the summation over the pulse index *n*, we arrive at

$$Z(u_v, u_s) = A_R W_{I_{TX}}\left(\frac{a_{wr}}{\rho_r}\left(u_s\delta_s - s_{r,0}\right)\right) W_N\left(\frac{a_{wv}}{\rho_v}\left(u_v\delta_v - v_{target}\right)\right), \tag{38}$$

where

a_{wv} = the normalized broadening factor for the mainlobe in velocity, and

$$\rho_v = \frac{a_{wv}\,\pi\,c\,f_p}{\omega_0 N} \text{ = velocity resolution.} \tag{39}$$

From this we observe the following.

- There is clearly a well-defined peak at indices that correspond to $s_{r,0}$ and v_{target}.
- Range sidelobes will extend in the direction of u_s.
- Velocity sidelobes will extend in the direction of u_v.

At this point we have created a 2-dimensional array where each array position corresponds to a unique combination of range and target velocity. Any clutter velocity due to radar motion has been compensated. In fact, even the range dependence of the clutter has been compensated. This means that target velocity is with respect to the center of the clutter band, even perhaps taking into account topographic variations as a function of range.

5 SUMMARY & CONCLUSIONS

We summarize herein the following.

- Backprojection is well established as a technique for SAR image formation.
- Backprojection may also be applied to forming a range-velocity map for GMTI target detection.
- Backprojection is effective in mitigating target migration through range resolution cells, due to both the radar's closing velocity with the surrounding clutter, and the target's own line-of-sight velocity with respect to the clutter.

ACKNOWLEDGEMENTS

Sandia National Laboratories is a multi-program laboratory managed and operated by Sandia Corporation, a wholly owned subsidiary of Lockheed Martin Corporation, for the U.S. Department of Energy's National Nuclear Security Administration under contract DE-AC04-94AL85000.

REFERENCES

[1] D. C. Munson, Jr., J. D. O'Brien, W. Jenkins, "A tomographic formulation of spotlight-mode synthetic aperture radar," *Proceedings of the IEEE* , vol.71, no.8, pp. 917-925, Aug. 1983.

[2] R. P. Perry, R. C. DiPietro, R. L. Fante, "SAR imaging of moving targets," IEEE Transactions on Aerospace and Electronic Systems, vol. 35, no. 1, pp. 188-199, January 1999.

[3] R. P. Perry, R. C. DiPietro, R. L. Fante, "Coherent Integration With Range Migration Using Keystone Formatting," Proceedings of the 2007 IEEE Radar Conference, pp. 863-868, 17-20 April 2007.

[4] Armin W. Doerry, "GMTI Processing using Back Projection," Sandia Report SAND2013-5111, Unlimited Release, July 2013.

[5] Armin W. Doerry, "Performance Limits for Exo-Clutter Ground Moving Target Indicator (GMTI) Radar", Sandia Report SAND2010-5844, Unlimited Release, September 2010.

[6] A. W. Doerry, E. Bishop, J. Miller, V. Horndt, D. Small, "Designing interpolation kernels for SAR data resampling", SPIE 2012 Defense, Security & Sensing Symposium, Radar Sensor Technology XVI, Vol. 8361, Baltimore MD, 23-27 April 2012.